

# Theoretical Lower Bound for Indoor Visible Light Positioning Using Received Signal Strength Measurements and an Aperture-Based Receiver

Heidi Steendam, *Senior Member, IEEE*, Thomas Qian Wang, and Jean Armstrong, *Fellow, IEEE*

**Abstract**—Indoor visible light positioning (VLP) using signals transmitted by lighting LEDs is a topic attracting increasing interest within the research community. In the recent years, VLP techniques using a range of receiver structures and positioning algorithms have been described. In this paper, we analyze the performance of a VLP system, which uses an aperture-based receiver and measurements of received signal strength. An aperture-based receiver has a number of receiving elements, each consisting of a photodiode and an associated aperture. It has been shown that receivers of this form can be designed which are compact and provide both a wide overall field-of-view and good angular diversity. As a result, they can efficiently extract position-related information from light transmitted by nondirectional LEDs. In our approach, we correlate the signals at the outputs of the photodiodes with a set of reference signals. The resulting observations include information on the received signal strength as well as the angle-of-arrival, and are used to directly estimate the receiver's position. In order to assess the performance of positioning algorithms based on this approach, we derive the Cramer–Rao lower bound on the position estimate. We show that the Cramer–Rao bound depends on the selected reference signal, and that subcentimetre to centimetre accuracy can be obtained, using only a limited number of nondirectional LEDs.

**Index Terms**—Cramer–Rao bound, positioning, VLP.

## I. INTRODUCTION

**D**URING the last decade, visible light communication (VLC) has received considerable attention in the research community, because it offers a low-cost alternative to traditional RF communication systems. The success of VLC is a consequence of the widespread deployment of white LEDs, which

due to their low cost and energy efficiency, are gradually replacing conventional fluorescent and incandescent lights. In contrast to conventional light sources, white LEDs can be modulated at frequencies up to several MHz, making high-speed data rate communication feasible [1]. Furthermore, VLC is a viable alternative for situations where traditional RF communication is not possible due to safety reasons, e.g. in hospitals. Recently, VLC has also been considered for indoor positioning [2]–[12].

Since the development of GPS technology, the number of applications that make use of the user's position has exploded. However, indoors the reception of the satellite signals is reduced. Therefore, from the beginning of this century, researchers have tried to develop a positioning system for indoor areas. However, an accurate low-cost energy-efficient solution is still lacking. Compared to RF positioning solutions, visible light positioning (VLP) has a number of advantages. Firstly, luminaires are generally placed at regular intervals on the ceiling, so most positions in the room experience line-of-sight (LOS). Secondly, because light is blocked by opaque walls, no interference from adjacent rooms will be present. Thirdly, the deployment cost of the VLP solution is low, because lighting must be provided anyway, and the hardware cost of a white LED and a photodiode (PD) is negligible. Hence, VLP should be considered as a viable candidate for indoor localization.

Several approaches exist for positioning using VLP. Some already deployed solutions, e.g. ByteLight and Philips GE, use the CCD camera available in a mobile phone. Because of the large number of pixels, the CCD camera can extract accurate information about the direction of arrival of the light. However, the sensor quickly drains the battery of a mobile phone and because of its low refresh rate, the light should be modulated at a low frequency, resulting in flicker. Therefore, many recent papers consider the use of a PD, e.g. [3]–[12]. These papers apply several approaches. Some papers consider a direct estimation of the position e.g. [11], and others use a two-step approach by first extracting distance information based on the received signal strength (RSS) e.g. [3], [5], [7]–[9], time-(difference-)of-arrival (T(D)OA) e.g. [4], [10] or angle-of-arrival (AOA) e.g. [6], [12], and use trilateration or triangulation to obtain the user's position in the second step. The resulting position accuracy ranges between several centimetres and a metre, depending on how much position-related information is extracted from the light. Most researchers obtain position-related information by using directional LEDs (e.g. with higher Lambertian order) and

Manuscript received January 26, 2016; revised July 3, 2016, August 26, 2016, and December 23, 2016; accepted December 23, 2016. Date of publication December 27, 2016; date of current version January 9, 2017. This work was supported in part by the Australian Research Council's Discovery funding schemes DP130101265 and DP150100003, and in part by the Interuniversity Attraction Poles Programme initiated by the Belgian Science Policy Office. The work of H. Steendam was supported by the Flemish Fund for Scientific Research.

H. Steendam is with the Digital Communications Research Group of the Telecommunications and Information Processing Department of Ghent University, Gent 9000, Belgium, on leave to Monash University, Melbourne, Vic 3800, Australia (e-mail: Heidi.Steendam@telin.ugent.be).

T. Q. Wang was with Monash University, Melbourne, Vic 3800, Australia. He is now with the University of Technology Sydney, Sydney, NSW 2007, Australia (e-mail: qian.wang@uts.edu.au).

J. Armstrong is with the Department of Electrical and Computer Systems Engineering, Monash University, Melbourne, Vic 3800, Australia (e-mail: Jean.Armstrong@monash.edu).

Color versions of one or more of the figures in this paper are available online at <http://ieeexplore.ieee.org>.

Digital Object Identifier 10.1109/JLT.2016.2645603

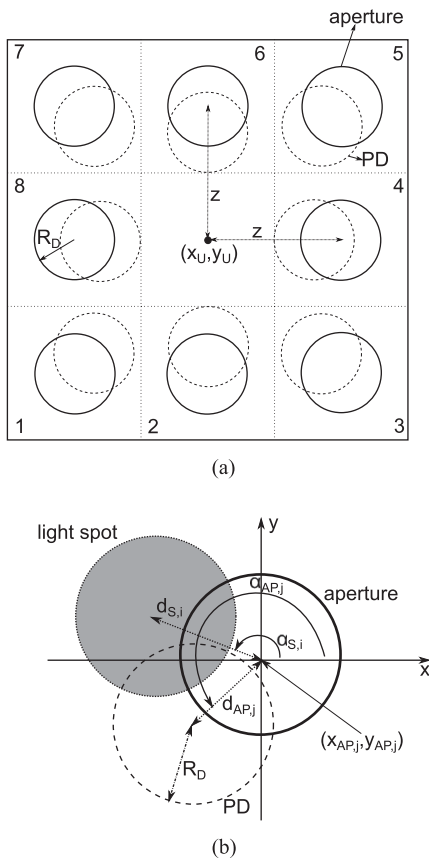


Fig. 1. (a) Top view of a receiver structure consisting of  $M = 8$  REs and (b) top view of one RE.

a non-directional receiver, but other solutions considering a directional receiver combined with non-directional LEDs (e.g. with low Lambertian order) also exist. In the first approach, by narrowing the half-angle of the LED, the positioning accuracy can be improved within the LED's half-angle. However, when the half-angle is too narrow, many LEDs are required to obtain good positioning accuracy over an entire room. To overcome this limitation, recently researchers started investigating directional receivers. In [6], [12], the authors considered tilted PDs, mounted on the corners of a cube. Although accurate 3D positioning is possible with this approach, its practical use is limited as the resulting receiver is not compact. In this paper, we will consider a different directional receiver, i.e. the receiver structure from [13] consisting of PDs combined with apertures. The advantage of this receiver compared to [6], [12] is its compactness. The positions of the apertures are selected to obtain good angular diversity, i.e., the light captured by a receiving element will strongly depend on the direction of the light, implying the differences in RSS at the different PDs offer information on the direction of the light.

Although the existing papers on VLP promise good positioning accuracy, it is not clear to what extent the proposed algorithms are optimal. A way to assess the performance of algorithms is the Cramer-Rao bound (CRB), which is a theoretical lower bound on the mean-squared error (MSE) of an unbiased estimator. Only a few papers are available focussing on the

CRB for VLP. In [14] and [15], the authors consider the CRB for directional LEDs and a non-directional receiver, based on RSS and AOA measurements, respectively, while [16] derives the CRB for a TOA approach. However, TOA requires accurate synchronization between the transmitted optical signals. In [17], we considered the receiver structure from [13], where we directly estimate the user's position based on the RSS values, and the CRB was derived for observations consisting of the time-average of the received signals. However, to distinguish between the time-averaged signals of the different LEDs, the LEDs must transmit signals that do not overlap in time, which will not only cause flicker, but also requires accurate time synchronization at the transmitters. Hence, the approach in [17] has its practical limitations.

In this paper, we use the same receiver structure as in [17], and consider the direct estimation of the position based on the RSS values. However, in contrast to [17], the RSS values are obtained by correlating the received signals with a number of reference signals related to the transmitted signals. By properly selecting the transmitted signals and the reference signals, we can distinguish between the different transmitted signals at the receiver, even if they are transmitted simultaneously. Hence, the LEDs may transmit continuously and no synchronization between the LEDs is required. In this paper, we derive the CRB for this approach, and evaluate the effect of different system parameters. We show that only a limited number of LEDs is required to achieve accurate positioning. Hence, as to obtain an illuminance of 500-700 lux in e.g. office spaces or supermarkets, a large number of LEDs is available, we only need a small subset of these luminaires for positioning purposes. This will reduce the installation cost of the positioning system. To assess the tightness of the CRB, which is derived for the case of a LOS link between the LEDs and the receiver only, we compare the results with the mean squared error (MSE) performance of the maximum likelihood (ML) estimator for the position, in the absence and presence of diffuse reflections of the light on walls and objects. We show that the MSE of the ML estimator closely matches the CRB and that if a diffuse component is present, the degradation of the MSE of the ML estimator only is substantial near the walls, indicating that the CRB is still a good lower bound if a diffuse component is present. In contrast to the ML estimator, where the performance must be evaluated through simulations because of the complex relationship between the receiver position and the received signal strengths, the CRB can be computed analytically with low complexity. Therefore the CRB derived in this paper is very useful for assessing and optimizing system performance. The approach in this paper outperforms the results from [17] and show that with realistic parameter settings, a position accuracy of a centimetre can be obtained.

## II. SYSTEM DESCRIPTION

### A. Received Signals

We consider the receiver introduced in [13], which contains  $M$  receiving elements (RE). Each RE consists of a bare, circular PD with radius  $R_D$  and an aperture, as shown in Fig. 1. The

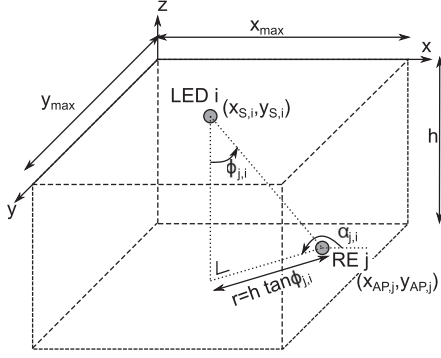


Fig. 2. The positions of LED  $i$  and RE  $j$  in the room, and the definition of the incident angle  $\phi_{j,i}$  and polar angle  $\alpha_{j,i}$ .

aperture is a circular hole with radius  $R_A$  in an opaque screen that is located in a plane that is parallel to the plane of the PDs, and located at height  $h_A$  above the plane of the PDs. We assume that the only light that reaches a PD is the light that passes through its aperture, and that the radius  $R_A$  of the aperture is large compared to the wavelength of the light. As a result, the incident light will introduce a circular light spot<sup>1</sup> on the plane of the PD [see Fig. 1(b)]. In the following, we assume  $R_A = R_D$ , as in that case a different position of the receiver will always result in different RSS values. In contrast, when  $R_A \neq R_D$ , the dependency of the RSS values on the position may show ambiguities, reducing the positioning accuracy.

To the ceiling of the room are attached  $K$  white LEDs at positions  $(x_{S,i}, y_{S,i})$ ,  $i = 1, \dots, K$ , which can be modelled as generalized Lambertian LEDs with order  $m_i$ . We assume the plane of the receiver is parallel to the ceiling, at a distance  $h$  below the ceiling, as shown in Fig. 2. Our goal is to estimate the position of  $(x_U, y_U)$ , which is a reference point on the receiver. In the system we consider, the apertures are symmetrically arranged around the reference point with the offset of the centre of the  $j$ th aperture  $(x_{AP,j}, y_{AP,j})$  from the reference point given by  $(\delta x_j, \delta y_j)$  so that  $(x_{AP,j}, y_{AP,j}) = (x_U + \delta x_j, y_U + \delta y_j)$ . To achieve angular diversity, each PD is also offset from its aperture. As shown in Fig. 1(b), the position of the PD is determined by the angle  $\alpha_{AP,j}$  and the distance  $d_{AP,j}$  between the centres of the aperture and the PD. The parameters  $(\delta x_j, \delta y_j)$  and  $(d_{AP,j}, \alpha_{AP,j})$  depend on the receiver layout. We will show that the received signal strength can be written as a function of the incident and polar angles  $(\phi_{j,i}, \alpha_{j,i})$  between LED  $i$  and RE  $j$ . Taking into account Fig. 2, the relation between  $(x_{S,i}, y_{S,i})$  and  $(x_{AP,j}, y_{AP,j})$  is given by

$$\begin{aligned} x_{S,i} &= x_{AP,j} + h \tan \phi_{j,i} \cos \alpha_{j,i} \\ y_{S,i} &= y_{AP,j} + h \tan \phi_{j,i} \sin \alpha_{j,i}. \end{aligned} \quad (1)$$

In the following, it will be shown that the RSS in a RE depends on the incident and polar angle. The angles  $(\phi_{j,i}, \alpha_{j,i})$  are

<sup>1</sup>The circular shape of the light spot is due to elementary geometry related to the intersection of elliptical cylinders and parallel planes. As the planes of the apertures and the PDs are parallel, the shapes and sizes of the intersections will be equal. Hence, as the aperture is circular with radius  $R_A$ , the light spot will also be circular with radius  $R_A$ .

deterministic functions of the positions of the apertures  $(x_{AP,j}, y_{AP,j})$  and the LEDs  $(x_{S,i}, y_{S,i})$  (1). The goal of this paper is to directly estimate the position  $(x_U, y_U)$  of the receiver, while the relative distances  $(\delta x_j, \delta y_j)$  of the apertures to the reference point on the receiver and the positions  $(x_{S,i}, y_{S,i})$  of the LEDs are known at the receiver. Hence, the angles  $(\phi_{j,i}, \alpha_{j,i})$  do not have to be determined by the receiver, but are only introduced to simplify the notations in the following.

The optical signal transmitted by LED  $i$  equals  $s_i(t)$ . At RE  $j$ , the optical signal coming from the different LEDs is converted to an electrical signal  $r_j(t)$  by the PD. This signal  $r_j(t)$  consists of a linear combination of the transmitted signals  $s_i(t)$ . To separate the contributions from the different LEDs, the receiver correlates the signal  $r_j(t)$  with a set of reference signals  $\{\psi_i(t) | i = 1, \dots, K\}$  over the time interval  $[0, T]$ , where reference signal  $\psi_i(t)$  is a function of the signal  $s_i(t)$  transmitted by LED  $i$ :  $r_i[j] = \int_0^T r_j(t) \psi_i(t) dt$ ,  $j = 1, \dots, M$ ,  $i = 1, \dots, K$ . Defining the  $MK \times 1$  vector  $\mathbf{r} = (\mathbf{r}_1^T \dots \mathbf{r}_K^T)^T$  as the vector of observations, with  $\mathbf{r}_\ell = (r_\ell[1] \dots r_\ell[M])^T$ , we obtain

$$\mathbf{r} = R_p \tilde{\mathbf{H}} \boldsymbol{\mu} + \tilde{\mathbf{n}}. \quad (2)$$

In (2),  $R_p$  is the responsivity of the PD and  $\tilde{\mathbf{H}}$  is a  $MK \times K^2$  matrix:

$$\tilde{\mathbf{H}} = \begin{pmatrix} \mathbf{H} & \mathbf{0} & \dots & \mathbf{0} \\ \mathbf{0} & \mathbf{H} & \dots & \mathbf{0} \\ \vdots & \vdots & \ddots & \vdots \\ \mathbf{0} & \mathbf{0} & \dots & \mathbf{H} \end{pmatrix} \quad (3)$$

with  $(\mathbf{H})_{j,i} = h_c^{(j,i)}$ ,  $j = 1, \dots, M$ ,  $i = 1, \dots, K$  the  $M \times K$  matrix of the channel gains. Further, the  $K^2 \times 1$  vector  $\boldsymbol{\mu}$  is a function of the transmitted optical signals  $s_i(t)$ ,  $i = 1, \dots, K$ , and is defined as  $\boldsymbol{\mu} = (\boldsymbol{\mu}_1^T \dots \boldsymbol{\mu}_K^T)^T$ , with  $\boldsymbol{\mu}_\ell = (\mu_\ell[1] \dots \mu_\ell[K])^T$  and  $\mu_\ell[i] = \int_0^T s_i(t) \psi_\ell(t) dt$ . The  $MK \times 1$  vector  $\tilde{\mathbf{n}} = (\mathbf{n}_1^T \dots \mathbf{n}_K^T)^T$ , with  $\mathbf{n}_\ell = (n_\ell[1] \dots n_\ell[M])^T$  is the contribution from the noise. The noise consists of shot noise and thermal noise. Assuming the bandwidth of the signals  $s_i(t)$  is below 10 MHz, in many practical situations, the noise will be dominated by the shot noise [18]. Hence, in the following, we will only consider the contribution from the shot noise. The shot noise is dominated by signal-independent background light, so  $\tilde{\mathbf{n}}$  can be modeled as zero-mean Gaussian random variables with covariance matrix  $\frac{N_0}{2} \tilde{\mathbf{R}}$ , where  $\tilde{\mathbf{R}} = \mathbf{R}_\psi \otimes \mathbf{I}_M$ , with  $\otimes$  denoting the Kronecker product of the  $K \times K$  matrix  $\mathbf{R}_\psi$  and the  $M \times M$  identity matrix  $\mathbf{I}_M$ , and  $(\mathbf{R}_\psi)_{\ell,\ell'} = \int_0^T \psi_\ell(t) \psi_{\ell'}(t) dt$ . Further, the noise level  $N_0$  is defined as  $N_0 = 2qR_p p_n A_D \Delta\lambda$ , where  $q$  is the charge of an electron,  $p_n$  is the background spectral irradiance,  $A_D$  is the area of the PD and  $\Delta\lambda$  is the bandwidth of the optical filter in front of the PD. Taking into account that the  $i$ th LED is modeled as a generalized Lambertian LED with order  $m_i$ , the channel gain  $h_c^{(j,i)}$  can be written as [18]

$$h_c^{(j,i)} = \frac{m_i + 1}{2\pi h^2} A_0^{(j,i)} \cos^{m_i+3} \phi_{j,i} \quad (4)$$

where  $A_0^{(j,i)}$  corresponds to the surface of the overlap area between PD  $j$  and the light spot originating from LED  $i$ :

$$A_0^{(j,i)} = \begin{cases} 2R_D^2 \arccos\left(\frac{d_{j,i}}{2R_D}\right) & 0 \leq d_{j,i} \leq 2R_D \\ -\frac{d_{j,i}}{2} \sqrt{4R_D^2 - d_{j,i}^2} & d_{j,i} > 2R_D \end{cases} \quad (5)$$

This overlap area is determined by the distance  $d_{j,i}$  between the centre of the light spot and the centre of the PD, which can be written as

$$\begin{aligned} d_{j,i} &= \left[ \left( d_S^{(j,i)} \cos \alpha_S^{(j,i)} - d_{AP,j} \cos \alpha_{AP,j} \right)^2 \right. \\ &\quad \left. + \left( d_S^{(j,i)} \sin \alpha_S^{(j,i)} - d_{AP,j} \sin \alpha_{AP,j} \right)^2 \right]^{1/2} \\ &= \left[ \left( \frac{h_A}{h} (x_{S,i} - x_{AP,j}) - d_{AP,j} \cos \alpha_{AP,j} \right)^2 \right. \\ &\quad \left. + \left( \frac{h_A}{h} (y_{S,i} - y_{AP,j}) - d_{AP,j} \sin \alpha_{AP,j} \right)^2 \right]^{1/2}. \quad (6) \end{aligned}$$

The angle  $\alpha_S^{(j,i)}$  and position  $d_S^{(j,i)}$  of the light spot are determined by the angle-of-incidence  $\phi_{j,i}$  and polar angle  $\alpha_{j,i}$  of the light arriving from LED  $j$  on PD  $i$ :  $d_S^{(j,i)} = h_A \tan \phi_{j,i}$  and  $\alpha_S^{(j,i)} = \pi + \alpha_{j,i}$ . Further, the second line in (6) is obtained by substituting (1).

### B. Cramer-Rao Bound

The mean-squared error (MSE) of any unbiased estimate  $\hat{\boldsymbol{\theta}} = (\hat{x}_U, \hat{y}_U)$  of the position  $\boldsymbol{\theta} = (x_U, y_U)$  based on the observation (2) is lower bounded by the CRB, defined as

$$\text{MSE} = E[(x_U - \hat{x}_U)^2 + (y_U - \hat{y}_U)^2] \geq \text{trace}(\mathbf{F}_U^{-1}). \quad (7)$$

In (7),  $\mathbf{F}_U$  is the Fisher information matrix (FIM) [19]:

$$\mathbf{F}_U = E \left[ (\nabla_{\boldsymbol{\theta}} \ln p(\mathbf{r}|\boldsymbol{\theta})) (\nabla_{\boldsymbol{\theta}} \ln p(\mathbf{r}|\boldsymbol{\theta}))^T \right]. \quad (8)$$

Bearing in mind that  $\mathbf{r}|\boldsymbol{\theta} \sim N(R_p \tilde{\mathbf{H}} \boldsymbol{\mu}, \frac{N_0}{2} \tilde{\mathbf{R}})$ , it is shown in the Appendix that

$$\mathbf{F}_U = \frac{2R_p^2}{N_0} \begin{bmatrix} Z^{x_U x_U} & Z^{x_U y_U} \\ Z^{y_U x_U} & Z^{y_U y_U} \end{bmatrix}. \quad (9)$$

In (9),  $Z^{ab}$ ,  $a, b \in \{x_U, y_U\}$  is defined as

$$Z^{ab} = \text{trace}(\mathbf{R}_{\psi}^{-1} \mathbf{W}^{ab}), \quad (10)$$

where  $(\mathbf{W}^{ab})_{\ell, \ell'} = \boldsymbol{\mu}_{\ell}^T \mathbf{X}^{ab} \boldsymbol{\mu}_{\ell'}$  and

$$\begin{aligned} (\mathbf{X}^{ab})_{i, i'} &= \left[ \left( \frac{\partial}{\partial a} \mathbf{H} \right)^T \left( \frac{\partial}{\partial b} \mathbf{H} \right) \right]_{i, i'} \\ &= \sum_{j=1}^M \frac{\partial}{\partial a} h_c^{(j,i)} \frac{\partial}{\partial b} h_c^{(j,i')}. \quad (11) \end{aligned}$$

In (11), it can be observed that in order to compute the CRB, we need the derivative of the channel gain  $h_c^{(j,i)}$  (4) with respect to  $x_U$  and  $y_U$ :

$$\begin{aligned} \frac{\partial}{\partial a} h_c^{(j,i)} &= \frac{m_i + 1}{2\pi h^2} \left[ \left( \frac{\partial}{\partial z} A_0^{(j,i)} \right) \cos^{m_i+3} \phi_{j,i} \right. \\ &\quad \left. + A_0^{(j,i)} \frac{\partial}{\partial z} \cos^{m_i+3} \phi_{j,i} \right] \quad (12) \end{aligned}$$

with  $a \in \{x_U, y_U\}$ . Taking into account (1), (5) and (6), it follows that

$$\begin{aligned} \frac{\partial}{\partial x_U} \cos^{m_i+3} \phi_{j,i} &= \frac{m_i + 3}{h^2} (x_{S,i} - x_{AP,j}) \cos^{m_i+5} \phi_{j,i} \\ \frac{\partial}{\partial y_U} \cos^{m_i+3} \phi_{j,i} &= \frac{m_i + 3}{h^2} (y_{S,i} - y_{AP,j}) \cos^{m_i+5} \phi_{j,i}. \quad (13) \end{aligned}$$

For  $0 \leq d_{j,i} \leq 2R_D$  and  $a \in \{x_U, y_U\}$ ,  $\frac{\partial}{\partial a} A_0^{(j,i)}$  yields

$$\frac{\partial}{\partial a} A_0^{(j,i)} = -\sqrt{4R_D^2 - d_{j,i}^2} \frac{\partial}{\partial a} d_{j,i} \quad (14)$$

and

$$\begin{aligned} \frac{\partial}{\partial x_U} d_{j,i} &= -\frac{R_D}{h d_{j,i}} \left( \frac{h_A}{h} (x_{S,i} - x_{AP,j}) + d_{AP,j} \cos \alpha_{AP,j} \right) \\ \frac{\partial}{\partial y_U} d_{j,i} &= -\frac{R_D}{h d_{j,i}} \left( \frac{h_A}{h} (y_{S,i} - y_{AP,j}) + d_{AP,j} \sin \alpha_{AP,j} \right). \quad (15) \end{aligned}$$

### C. Transmitted Optical Signals

The CRB depends on the transmitted optical signals  $s_i(t)$  and reference signals  $\psi_{\ell}(t)$  through the vector  $\boldsymbol{\mu}_{\ell}$  and the matrix  $\mathbf{R}_{\psi}$ . To assess the effect of  $s_i(t)$  and  $\psi_{\ell}(t)$ , we consider the following transmitted optical signals  $s_i(t)$ . Taking into account that the transmitted optical signals must be real-valued and positive, we assume the transmitted optical signal is a dc-biased windowed sinusoid waveform with duration  $T$ :

$$s_i(t) = A_i w(t) (1 + \cos(2\pi f_{c,i} t)) \quad (16)$$

where the window function  $w(t)$  has no contributions outside the interval  $[0, T]$ :  $w(t) = 0$  for  $t \notin [0, T]$ . We denote  $A_i w(t)$  the dc component and  $A_i w(t) \cos(2\pi f_{c,i} t)$  the carrier component of the signal. Further, the frequency  $f_{c,i}$  of the sinusoid is assumed to have an integer number of periods within the interval  $[0, T]$ , and the frequencies corresponding to the different LEDs are orthogonal over  $[0, T]$ , i.e.  $(f_{c,i} - f_{c,i'})T$  is integer for  $i, i' = 1, \dots, K$ . The selection of the frequencies can be based on the discrete Fourier transform, resulting in orthogonal frequency division multiplexing (OFDM), which is commonly considered for optical wireless communication [20]–[23]. The window-function is a smooth function, e.g. a raised cosine window:

$$w(t) = \left( 1 + \cos \left( \frac{2\pi}{T} \left( t - \frac{T}{2} \right) \right) \right). \quad (17)$$

Further, the window function  $w(t)$  is assumed to have a narrow bandwidth compared to the frequencies  $f_{c,i}$  of the sinusoids.

Taking into account (16) and (17), the optical power transmitted by LED  $i$  equals:

$$P_{opt,i} = \frac{1}{T} \int_0^T s_i(t) dt = A_i. \quad (18)$$

For the reference signals  $\psi_\ell(t)$ , we consider two different cases. In the first case, we select reference signal  $i$  to be the entire transmitted optical signal transmitted by LED  $i$ , i.e.  $\psi_i(t) = s_i(t)$ . In that case, it can be verified that  $\mathbf{R}_\psi = (\boldsymbol{\mu}_1 \dots \boldsymbol{\mu}_K)$ . As a result, the matrix  $\mathbf{W}^{ab}$  can be rewritten as  $\mathbf{W}^{ab} = \mathbf{R}_\psi^T \mathbf{X}^{ab} \mathbf{R}_\psi$ , so that the elements  $Z^{ab}$  (10) reduce to  $Z^{ab} = \text{trace}(\mathbf{R}_\psi \mathbf{X}^{ab})$ , where we used  $\mathbf{R}_\psi^T = \mathbf{R}_\psi$ . By substituting (16) and (17) in  $\mathbf{R}_\psi$ , we obtain

$$Z_1^{ab} = \text{trace}(\mathbf{R}_{s,1} \mathbf{X}^{ab}), \quad (19)$$

where  $\mathbf{R}_{s,1} = \frac{3T}{2} (\mathbf{A}^T \mathbf{A} + \frac{1}{2} \text{diag}(\mathbf{A} \circ \mathbf{A}))$ , with  $\mathbf{A} = (A_1 \dots A_K)$  is the vector of transmitted optical powers,  $\circ$  denotes the Hadamard product, and  $\text{diag}(\mathbf{A})$  is the diagonal matrix with as diagonal elements the elements of  $\mathbf{A} \circ \mathbf{A}$ .

As can be observed, by correlating the received signal  $r_j(t)$  with the entire transmitted optical signals  $s_i(t)$ , the different components of the resulting observation are correlated, i.e.  $\mathbf{R}_\psi = \mathbf{R}_{s,1}$  is not a diagonal matrix. This correlation is due to the presence of the dc component of  $s_i(t)$  in the reference signals. As this correlation will make it harder to separate the contributions from the different LEDs, we consider the second case, where the reference signal  $\psi_i(t)$  does not contain the dc component from  $s_i(t)$ :  $\psi_i(t) = A_i w(t) \cos(2\pi f_{c,i} t)$ ,  $i = 1, \dots, K$ . In that case,  $\boldsymbol{\mu}_\ell$  and  $\mathbf{R}_\psi$  reduce to

$$\begin{aligned} \boldsymbol{\mu}_\ell[i] &= \frac{3T}{4} A_i A_\ell \delta_{i,\ell} \\ \mathbf{R}_\psi &= \frac{3T}{4} \text{diag}(\mathbf{A} \circ \mathbf{A}). \end{aligned} \quad (20)$$

Inspecting (20) reveals that in this case, again  $\mathbf{R}_\psi = (\boldsymbol{\mu}_1 \dots \boldsymbol{\mu}_K)$ , so that  $Z^{ab}$  can be rewritten as

$$Z_2^{ab} = \text{trace}(\mathbf{R}_{s,2} \mathbf{X}^{ab}), \quad (21)$$

where  $\mathbf{R}_{s,2} = \mathbf{R}_\psi = \frac{3T}{4} \text{diag}(\mathbf{A} \circ \mathbf{A})$ .

### III. NUMERICAL RESULTS

In the evaluation of the CRB, we consider the receiver structure shown in Fig. 1(a). The receiver consists of  $M = 8$  REs, where the relative positions  $(\delta x_j, \delta y_j)$  of the apertures with respect to the position  $(x_U, y_U)$  of the receiver are given by

$$\begin{aligned} \delta x_j &= \epsilon_{x,j} \cos \chi - \epsilon_{y,j} \sin \chi \\ \delta y_j &= \epsilon_{x,j} \sin \chi + \epsilon_{y,j} \cos \chi \end{aligned} \quad (22)$$

where  $\boldsymbol{\epsilon}_x = \epsilon R_D (-1 \ 0 \ 1 \ 1 \ 1 \ 0 - 1 - 1)$  and  $\boldsymbol{\epsilon}_y = \epsilon R_D (-1 - 1 - 1 \ 0 \ 1 \ 1 \ 1 \ 0)$ . The angle  $\chi$  in (22) expresses the orientation of the receiver in the  $(x, y)$ -plane, while the parameter  $\epsilon$  determines the distance between the apertures and the central point  $(x_U, y_U)$  of the receiver. In this paper, we restrict our attention to the case where the receiver is positioned in the  $(x, y)$ -plane, i.e., the plane

parallel to the ceiling where the LEDs are located.<sup>2</sup> Further, the PDs are placed at positions  $d_{AP,j} = \zeta R_D$  and  $\alpha_{AP,j} = j \frac{\pi}{4}$  relative to their apertures, where  $\zeta$  determines the field-of-view of the receiver and the angles  $\alpha_{AP,j}$  are selected to offer good angular diversity [13].

Unless stated otherwise, the  $K = P^2$  LEDs are uniformly placed on the ceiling according to a rectangular pattern at the positions  $x_S(i) = \frac{x_{\max}}{2P} + (i-1)_P \frac{x_{\max}}{P}$  and  $y_S(i) = \frac{y_{\max}}{2P} + \lfloor \frac{i-1}{P} \rfloor \frac{y_{\max}}{P}$ ,  $i = 1, \dots, K$ , where  $x_{\max}$  and  $y_{\max}$  are the length and width of the considered area,  $(x)_P$  is the modulo- $P$  operation of  $x$ , and  $\lfloor x \rfloor$  is the largest integer not exceeding  $x$ . Unless mentioned otherwise, we assume the LEDs have a non-directional radiation pattern, i.e. they can be modeled as Lambertian with order  $m_i = 1$ . Further, we assume the ceiling is at a height  $h = 2$  m above the receiver. In order to determine the shot noise power spectral density  $N_0 = 2qR_p p_n A_D \Delta\lambda$ , we assume a background spectral irradiance  $p_n = 5.8 \times 10^{-6}$  W/cm<sup>2</sup>·nm, a value that is commonly used in the literature [18]. Further, the PD has a radius  $R_D = 1$  mm and responsivity  $R_p = 0.4$  mA/mW [25]. The optical filter passes only visible light frequencies corresponding to 380 to 740 nm, resulting in an optical bandwidth of  $\Delta\lambda = 360$  nm. The resulting noise spectral density equals  $N_0 = 8.4 \times 10^{-24}$  A<sup>2</sup>/Hz. We assume the LEDs have the same transmit power (18):  $P_{opt,i} = A_i = A$ ,  $i = 1, \dots, K$ . In that case,  $\mathbf{A}^T \mathbf{A} = A^2 \mathbf{E}_K$  and  $\mathbf{A} \circ \mathbf{A} = A^2 \mathbf{I}_K$ , where  $\mathbf{E}_K$  is the  $K \times K$  matrix of all ones, and  $\mathbf{I}_K$  is the  $K \times K$  identity matrix. Inspecting (9), (19) and (21), it can be observed that the FIM is proportional to the ratio  $\gamma$ :

$$\gamma \triangleq 2TA^2 R_p^2 / N_0, \quad (23)$$

which is related to the signal-to-noise ratio.<sup>3</sup> Hence, the CRB will be inversely proportional to the length  $T$ . In the following, we assume the transmitted optical power of the non-directional LEDs with Lambertian order  $m_i = 1$  equals  $A = 1$  W.

We first evaluate the square root of the CRB (rCRB) as function of the position  $(x_U, y_U)$  of the receiver. In Fig. 3, the rCRB is shown for the two cases from Section II-C, for  $K = 4, 9$  and  $16$  and  $10 \log_{10} \gamma = 195.81$  dB, corresponding to a time window  $T = 1$  ms. We also show the rCRB from [17]. As expected, the value of the rCRB depends on the position of the receiver. In a large part of the considered  $10 \text{ m} \times 10 \text{ m}$  area, the rCRB is relatively constant, but near the edges of the area, the rCRB increases, for all three cases. This is expected, as near the edges of the area, the receiver captures less light compared to the middle

<sup>2</sup>A tilt of the receiver will have a deterministic effect on the RSS values. In mobile devices, inertial measurement units (IMUs) are available such as an accelerometer, gyroscope and compass. These IMUs are able to accurately determine the orientation of the mobile device. Hence, the orientation of the receiver is prior known, and can be incorporated in the positioning process. In [24], the authors used this prior knowledge on the tilt to compensate it and investigate its effect on the positioning performance. Their conclusion is that after compensation of the tilt, the performance degradation is marginal. As a tilt in our system has a similar effect on the RSS values compared to [24], we can extrapolate the results from [24] to our system and conclude that the orientation of the receiver will have a marginal effect on the positioning performance only, as long as the REs have a LOS connection with the LEDs.

<sup>3</sup>The signal-to-noise ratio is defined as the ratio of the received useful power to the received noise power, i.e.  $\text{SNR} = 2TA^2 (h_c^{(j,i)})^2 R_p^2 / N_0 = \gamma (h_c^{(j,i)})^2$

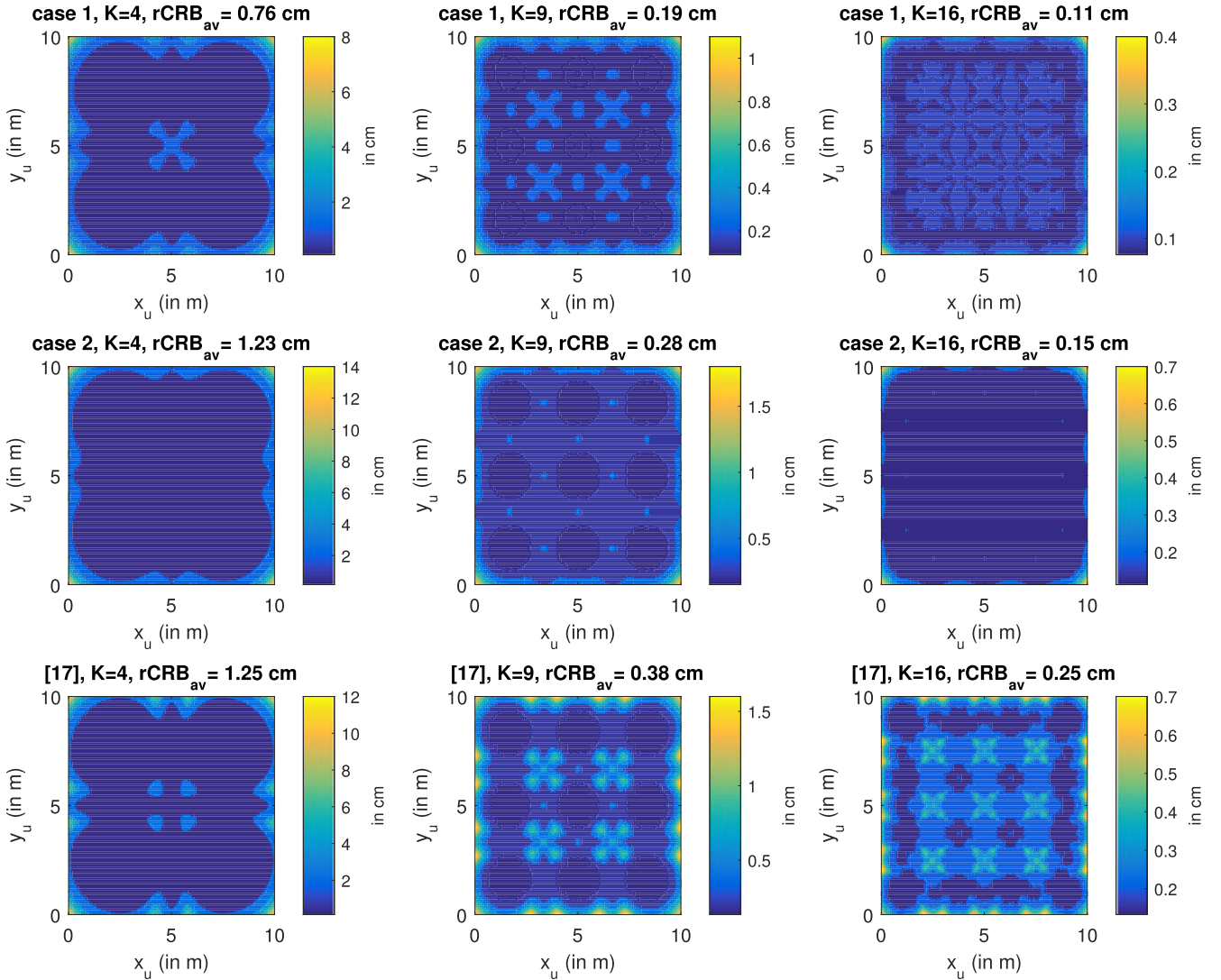


Fig. 3. Square root of the CRB as function of the position  $(x_U, y_U)$  of the receiver in the room, for  $10 \log_{10} \gamma = 195.81$  dB,  $x_{\max} = y_{\max} = 10$  m,  $\epsilon = 5$ ,  $h_A = R_D$ ,  $\chi = 0^\circ$  and  $\zeta = 0.5$ .

of the area, due to the directionality of the REs in the receiver [13] and the radiation pattern of the LEDs. Comparing the spatial average of the rCRB ( $r\text{CRB}_{\text{av}}$ ) for the three cases, i.e. the average over all positions in the area, we observe that Case 1 offers the highest accuracy, followed by Case 2 and the rCRB from [17] gives the lowest accuracy. This can be explained as in Case 1, the received signal  $r_j(t)$  is correlated with the entire transmitted signal  $s_i(t)$ , while in Case 2, by correlating with the carrier component only, we remove the dc-components from the received signal. Similarly, for the approach from [17], where the received signal  $r_j(t)$  is time-averaged over the interval  $[0, T]$ , we remove the carrier components from the signal and keep only the dc-components of the signal. Hence, Case 1 uses most of the information. Comparing the three cases, however, reveals that the reduction of the accuracy is moderate. Further, in the figure, we observe that the average rCRB decreases for an increasing number of LEDs.

Next, we evaluate the influence of the receiver layout and the orientation of the receiver. Our simulations showed that neither

the relative distance  $\epsilon$  of the apertures w.r.t. the centre of the receiver, nor the orientation  $\chi$  of the receiver have a noticeable influence on the performance. The independence of the performance to  $\epsilon$  suggests that other configurations of the REs, e.g. by placing the REs on a line, will not affect the positioning ability. Further, the independence of the rCRB to the orientation  $\chi$  can be attributed to the angular symmetry of the relative positions of the PDs with respect to their apertures, i.e., the angles  $\alpha_{AP,j}$  are uniformly distributed over the interval  $[0, 2\pi]$ . However, the performance will strongly depend on the relative distance  $\zeta R_D$  of the PDs w.r.t. their apertures, as this influences both the angular diversity and the field-of-view of the receiver, as well as the area of the PD, as this determines the amount of light captured by the receiver. First, we look at the effect of  $\zeta$ . In Fig. 4, we show the spatial average of the rCRB as function of  $\zeta$ . When  $\zeta$  is small, all REs will approximately receive the same amount of light, independent of the position of the receiver, i.e., although the receiver has the largest field-of-view, the angular diversity in the receiver is small. Hence, minimal information can be obtained

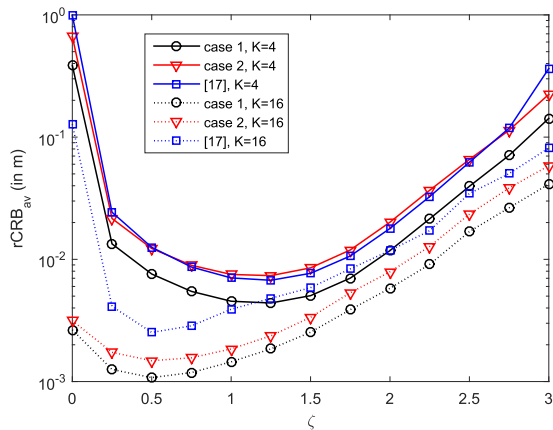


Fig. 4. Spatial average of rCRB as function of the relative distance  $\zeta$  of the PDs w.r.t. their apertures, for  $10 \log_{10} \gamma = 195.81$  dB,  $\epsilon = 5$ ,  $h_A = R_D$ ,  $\chi = 0^\circ$  and  $x_{\max} = y_{\max} = 10$  m.

about the polar angle  $\alpha_{j,i}$ , resulting in a lower accuracy. By increasing  $\zeta$ , the receiver will exhibit a larger angular diversity, i.e., the light captured by a RE strongly depends on the direction of the light. Moreover, by increasing  $\zeta$ , the receiver can detect larger incident angles, so that positions far away can better be determined. However, this comes at the cost of a slightly reduced field-of-view, as for small incident angles less light will be captured by the REs, resulting in a deterioration of the accuracy. The optimum value of  $\zeta$  is in the range  $\zeta \in [0.5, 1.5]$ . This optimum value reduces when the number of LEDs increases. This can be explained as follows. When  $K$  is small, despite the uniform placement of the LEDs at the ceiling, the incident angle  $\phi_{j,i}$  for the edges of the area is relatively large. Hence, to receive sufficient light for positioning at these positions,  $\zeta$  must be sufficiently large. When  $K$  is large, the distance between the receiver and the nearest LED becomes smaller, resulting in a smaller incident angle, even near the edges of the area. Hence, the value of  $\zeta$  can reduce. Secondly, we evaluate the effect of the height  $h_A$  on the average of the rCRB over all positions in a  $10 \text{ m} \times 10 \text{ m}$  area, assuming the relative positions of the photodiodes with respect to their apertures are fixed, i.e.  $\zeta$  is fixed. As can be observed in Fig. 5, the bound increases as function of  $h_A$ . This can be explained as follows. By changing the height  $h_A$ , the field-of-view of the receiver alters. For decreasing  $h_A$ , the field-of-view will become larger, so that, especially for positions at the edges of the area, the bound improves as more light will be received by the photodiodes. However, this effect is moderate: decreasing  $h_A$  will only result in a slight improvement of the bound. When  $h_A > R_D$ , the bound increases significantly due to the reduction of the field-of-view. When  $h_A$  is too large ( $h_A > 1.3R_D$  in Fig. 5), positions near the edges of the area will receive insufficient light to accurately determine their position because of this smaller field-of-view, resulting in an ill-conditioned FIM (9). Although the reduction of the field-of-view can be counteracted by increasing the distance between the photodiodes and their apertures, this will result in a larger receiver. For a compact receiver, the distance  $h_A$  therefore must be  $h_A \leq R_D$ . Thirdly, we investigate the effect of the area of

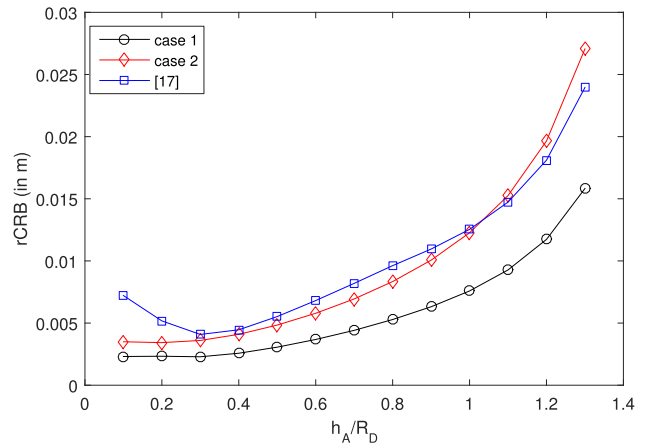


Fig. 5. Influence of the height  $h_A$  on  $r\text{CRB}_{\text{av}}$ ,  $10 \log_{10} \gamma = 195.81$  dB,  $K = 4$ ,  $x_{\max} = y_{\max} = 10$  m and  $\zeta = 0.5$ .

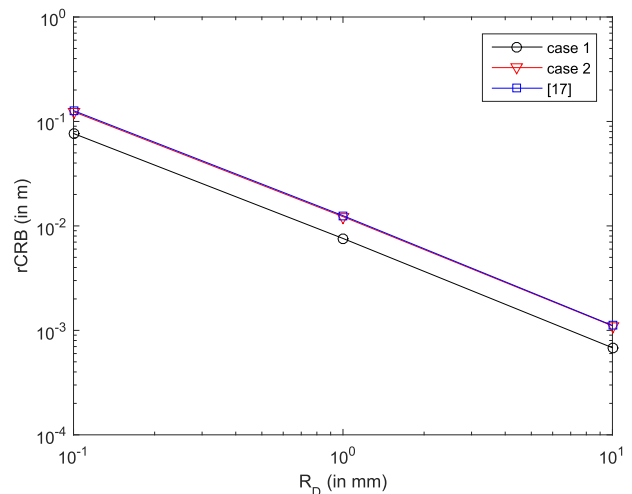


Fig. 6. Influence of the area of the PD on  $r\text{CRB}_{\text{av}}$ ,  $10 \log_{10} \gamma / R_D^2 = 255.81$  dB  $\text{m}^{-2}$ ,  $K = 4$ ,  $x_{\max} = y_{\max} = 10$  m,  $h_A = R_D$  and  $\zeta = 0.5$ .

the PD. The dependency of the spatial average of rCRB on the radius  $R_D$  of the PD is shown in Fig. 6. The rCRB is inversely proportional to  $R_D$ , or the square root of the PD area. Inspecting the elements of the FIM (9), we see that both the noise level  $N_0$  and the channel gain  $h_c^{(j,i)}$  are proportional to  $R_D^2$ , the latter through the area of overlap  $A_0^{(j,i)}$  (5) between the light spot and the PD. Hence, the elements of the FIM are proportional to  $R_D^2$ . Taking into account the results from Figs. 4–6, we can conclude that excellent positioning accuracy can be obtained in a  $10 \text{ m} \times 10 \text{ m}$  area with only four 1 W LEDs using a compact receiver.

In Fig. 7 we study the rCRB when the spacing between the LEDs changes. To this end, we consider a  $10 \text{ m} \times 10 \text{ m}$  area, where four 1 W LEDs are placed in a square grid with edge side  $\Delta$ , i.e. the LEDs have positions  $(5 \text{ m} - \Delta/2, 5 \text{ m} - \Delta/2)$ ,  $(5 \text{ m} - \Delta/2, 5 \text{ m} + \Delta/2)$ ,  $(5 \text{ m} + \Delta/2, 5 \text{ m} - \Delta/2)$  and  $(5 \text{ m} + \Delta/2, 5 \text{ m} + \Delta/2)$ . We show in the figure the probability of the rCRB being smaller than  $u$  for different spacings  $\Delta$ . As can be observed, the best performance is obtained when the spacing is

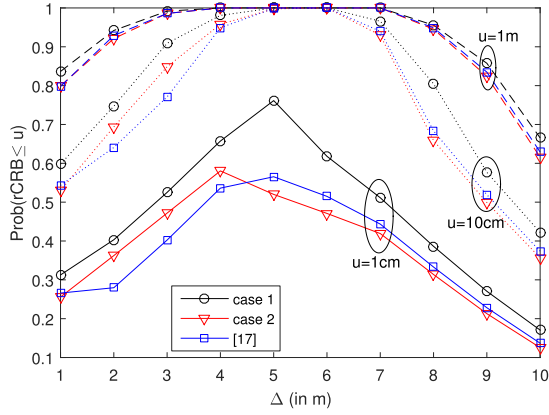


Fig. 7. Influence of the spacing of the LEDs on rCRB,  $10 \log_{10} \gamma = 195.81$  dB,  $K = 4$  and  $\zeta = 0.5$ .

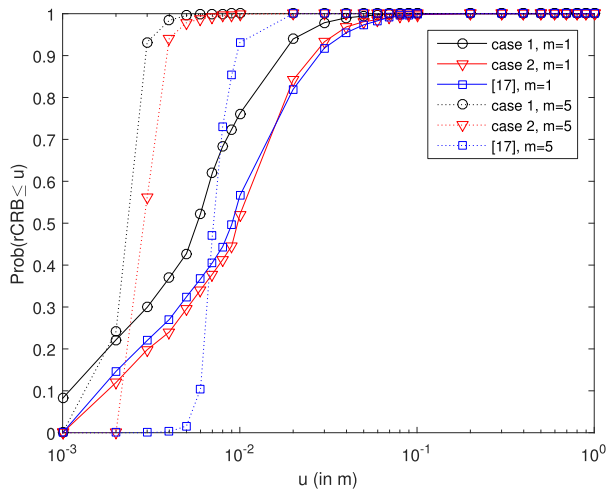


Fig. 8. Influence of the Lambertian order of the LEDs,  $10 \log_{10} \gamma / A^2 = 195.81$  dB,  $\zeta = 0.5$ .

around 5 m, i.e. when the LEDs are uniformly distributed over the area. This can be explained as follows. When the spacing is small, not only the distance between the LEDs and the positions at the boundaries of the considered area grows, but also the incident angles are relatively large. As a consequence, the received signal strengths for these positions will reduce resulting in a worse performance. On the other hand, when the spacing between the LEDs is large, e.g. when the LEDs are placed in the corners of the area, the positions in the center of the area will have lower performance, because of the large distance to the LEDs and the large incident angles. Hence, we can conclude that the best positioning performance will occur when the LEDs are distributed as uniformly as possible over the area. Further, we can conclude that centimetre accuracy can be obtained if one 1 W LED per  $25 \text{ m}^2$  is used for positioning.

Until now, we concentrated on the case where non-directional LEDs are used for positioning. Although most light sources for illumination are non-directional, corresponding to a Lambertian order  $m_i = 1$ , in some situations directional light sources with higher Lambertian order are used. Hence, we look at the effect of the directionality of the source. In Fig. 8, the probability of

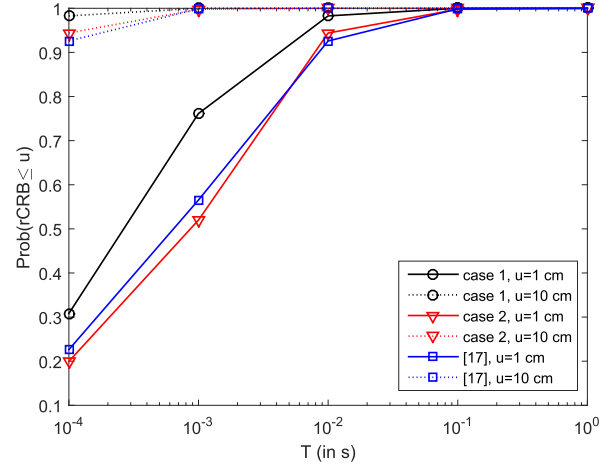


Fig. 9. Influence of the correlation time  $T$  on rCRB,  $10 \log_{10} \gamma / R_D^2 = 225.81$  dB  $\text{s}^{-1}$ ,  $K = 4$ ,  $x_{\max} = y_{\max} = 10$  m, and  $\zeta = 0.5$ .

the rCRB being smaller than  $u$  is shown as function of  $u$  for two cases. In the first case, four non-directional  $A = 1$  W LEDs with  $m_i = 1$  are attached to the ceiling of a  $10 \text{ m} \times 10 \text{ m}$  area, whereas in the second case, directional LEDs with  $m_i = 5$  are used. To allow for a fair comparison, we consider the case where the illuminance of the area is the same for both cases. Taking into account that for  $m_i = 1$ , the semi-angle of the LED is  $60^\circ$ , whereas for  $m_i = 5$ , this semi-angle is  $30^\circ$ , we need 36 directional  $A = 1/9$  W LEDs to have roughly the same illuminance. As can be observed in the figure, the performance is improved in the case of the directional LEDs, and the resulting positioning accuracy is also more uniform over the area, i.e. the curves for  $m_i = 5$  are steeper than for  $m_i = 1$ . This performance improvement can be explained by the reduction of the relative distance between a position in the area and the LEDs, and the presence of more signals to determine the position, although the optical power per LED is reduced. We can conclude that, the more uniformly spaced LEDs we use for positioning, the more uniform the positioning error over the area will be.

Next, the influence of the duration  $T$  of the correlation is shown in Fig. 9. The figure shows the probability of the rCRB being smaller than  $u$ , assuming four 1 W LEDs are used for positioning in a  $10 \text{ m} \times 10 \text{ m}$  area. Using a  $T = 1$  ms interval, more than half of the positions exhibits a position accuracy of better than 1 cm, and in all positions the error is smaller than 10 cm. By increasing the correlation interval to 10 ms, we can increase the accuracy so that even in more than 90% of the positions, an error smaller than 1 cm can be obtained. Hence, taking into account the excellent accuracy corresponding to a short correlation time, we conclude that with our approach, real-time positioning is possible.

Finally, we compare the rCRB with the root of the MSE (rMSE) of the ML estimator for  $(x_U, y_U)$ . The ML estimator reduces to

$$(\hat{x}_U, \hat{y}_U) = \arg \min_{(x_U, y_U)} \|\mathbf{r} - R_p \tilde{\mathbf{H}} \boldsymbol{\mu}\|^2. \quad (24)$$

The cost function to be minimized is a complex function of the receiver position, so that no closed-form expression for the ML

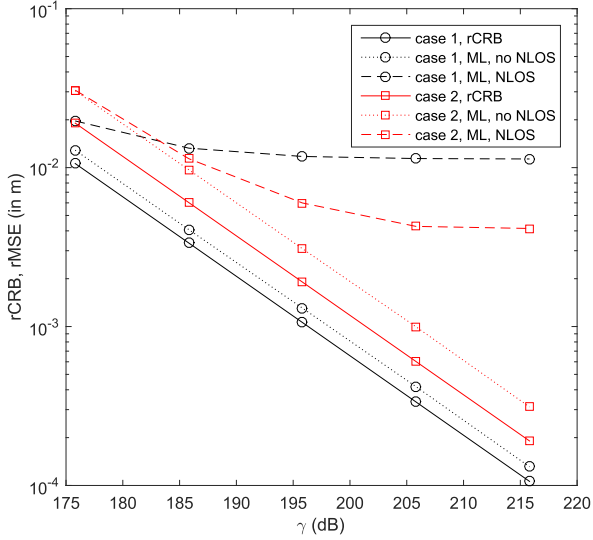


Fig. 10. Comparison of  $rMSE_{ML}$  and  $rCRB$ ,  $K = 4$ ,  $x_{\max} = y_{\max} = 5$  m,  $h_A = R_D$ ,  $\zeta = 0.5$  and  $\rho = 0.5$ .

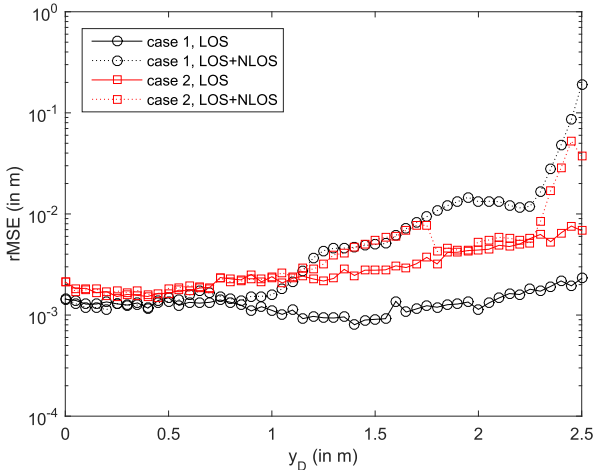


Fig. 11.  $rMSE_{ML}$  with and without diffuse component as function of the position  $y_D$  (with  $x_D = 0$ ),  $\gamma = 195.81$  dB,  $K = 4$ ,  $x_{\max} = y_{\max} = 5$  m,  $h_A = R_D$ ,  $\zeta = 0.5$  and  $\rho = 0.5$ .

estimate can be obtained. However, it can be verified that the cost function is well behaved and has a single minimum. To simulate the performance of the ML estimator, we use the Optimization Toolbox from Matlab to find  $(\hat{x}_{U,ML}, \hat{y}_{U,ML})$ , and compute the root of the MSE on the position,  $rMSE_{ML} = (E[(x_U - \hat{x}_{U,ML})^2 + (y_U - \hat{y}_{U,ML})^2])^{1/2}$ . The  $rMSE$ , averaged over all positions in a  $5\text{ m} \times 5\text{ m}$  room, is shown in Fig. 10 as function of the ratio  $\gamma$  (23), which is proportional to the signal-to-noise ratio, together with the corresponding  $rCRB$ . We consider two situations. In the first situation, only a LOS component is considered, i.e. no reflections are present, whereas in the second situation, also a diffuse channel component is present, due to reflections of the signals on the walls. The diffuse component will introduce an additional term  $R_p \tilde{\mathbf{H}}_{NLOS} \boldsymbol{\mu}$  in (2), i.e.

$$\mathbf{r} = R_p \tilde{\mathbf{H}} \boldsymbol{\mu} + R_p \tilde{\mathbf{H}}_{NLOS} \boldsymbol{\mu} + \tilde{\mathbf{n}} \quad (25)$$

where  $(\tilde{\mathbf{H}}_{NLOS})_{j,i} = h_{c,NLOS}^{(j,i)}$ . We simulated the diffuse channel gain  $h_{c,NLOS}^{(j,i)}$  by dividing the reflecting surfaces into small areas and calculating the light received by each small area from a given LED. The area was then considered as a Lambertian transmitter [18] with total transmit power proportional to the received power and the reflectivity of the surface. The power received by a given RE from this Lambertian transmitter was calculated using (4)–(6). The total diffuse component was calculated by summing the contributions from all reflecting surfaces. We took into account the first order reflections only. Following [26], a reflection coefficient  $\rho = 0.5$  was used for the walls. When only a LOS component is present, the performance of the ML estimator is close to the CRB, which indicates the CRB is a valuable tool for evaluating the performance if only a LOS component is present. For the case where a diffuse component is present, we use the ML estimator (24), which does not take into account the presence of a diffuse component  $\tilde{\mathbf{H}}_{NLOS}$  in the computation of  $R_p \tilde{\mathbf{H}} \boldsymbol{\mu}$ .<sup>4</sup> As can be observed, the performance of the estimator shows an error floor for large  $\gamma$ . The error floor for case 1 is larger than for case 2. To further investigate this error floor, we show in Fig. 11 the  $rMSE$  of the ML estimator with and without diffuse component, as function of  $y_D$ , for  $x_D = 0$ , where  $(x_D, y_D) = (0, 0)$  is the center of the room. As can be observed in the figure, the  $rMSE$  curves with and without diffuse component are very close in the middle of the room, as long as the position of the receiver is within the square with as corner points the LEDs (i.e.  $y_D < 1.25$  m). This can be explained as follows. Within this square, the LOS components of all REs and LEDs are sufficiently large, whereas the diffuse component is small as the receiver is far from the walls. The closer the receiver is to a wall, the larger the diffuse component due to that wall will be, while the LOS component to the LEDs that are furthest away reduces, due to the directivity of the REs. Hence, for these LEDs, the diffuse component will become dominant for some of the REs. In case 1, the RSS values corresponding to the different LEDs are correlated, i.e. the matrix  $\mathbf{R}_s$  is not diagonal. Hence, the adverse effect of the dominant diffuse component for the LEDs that are further away from the receiver will also affect the RSS values from the nearby LEDs. Because in case 2, the contributions from the different LEDs are uncorrelated (i.e.  $\mathbf{R}_s$  is diagonal), the adverse effect of the dominant diffuse component will not affect the contributions from the nearby LEDs, so the performance degradation for case 2 is smaller. For case 2, only when the receiver is very close to the wall, the performance degradation is substantial, although the resulting positioning error is smaller than 10 cm. Hence, even in the presence of diffuse reflection of the light, centimetre accuracy can be obtained. Our

<sup>4</sup>The diffuse component depends on the positions of the LEDs and the receiver w.r.t. the walls, as well as on the angle-of-arrival of a reflection arriving at the receiver. The ML estimator that takes into account the presence of the position-dependent diffuse component requires the prior knowledge of the dependency of the diffuse component to the position. However, as no simple but accurate analytical model for this diffuse component as function of the position and the angle-of-arrival exists, the ML estimator that is optimal for the case with diffuse component, i.e. that uses the knowledge of the dependency of the diffuse component  $\tilde{\mathbf{H}}_{NLOS}$  on the position of the receiver and the angle-of-arrival of a reflection in the computation of  $R_p \tilde{\mathbf{H}} \boldsymbol{\mu}$  in (24), cannot be derived.

results show that, for most positions in the room, the gap between the MSE of the ML estimator and the CRB is small. This indicates that the CRB, which was derived for the case of a LOS component only, is still a suitable lower bound on the performance even if diffusion, due to reflections on the walls and objects, is present. As the computational complexity of the CRB is much lower than simulating the ML estimator performance, the CRB is well suited to evaluate the efficiency of practical estimators and optimize the system parameters.

#### IV. CONCLUSIONS & DISCUSSION

In this paper, we investigate the Cramer-Rao bound for positioning using visible light. In contrast to other works dealing with the Cramer-Rao bound for visible light positioning, we consider a directional receiver [13] combined with non-directional LEDs. In our approach, we correlate the outputs of the PDs with a set of reference signals related to the signals transmitted by the LEDs, in order to separate the contributions from the different LEDs. Based on the resulting observations, the CRB on the position error is determined. This CRB depends on the transmitted signals and the reference signals. Therefore, we consider two different cases, where in the first scenario, the received signal is correlated with the transmitted optical signals, and in the second scenario, the dc-component is removed from the received signals. The CRB is compared with the MSE of the ML estimator, and it is shown that the MSE closely matches the CRB. The CRB, which was derived for the case of a LOS component only, is still a good lower bound for the case where diffuse reflections, due to reflections of the light on walls or objects, are present, except for positions near these walls. Further, the CRB can be computed with low complexity, in contrast to the evaluation of the performance of the ML estimator. This illustrates the relevance of the CRB. Further, we compare the results with the CRB derived in [17]. The first scenario gives the better performance, as all available information is used, and outperforms [17], where only the dc-component is kept. Our numerical results show that accurate real-time positioning is possible with a compact directional receiver, using only a limited number of LEDs per room. As a rule of thumb, we found that one LED per 25 m<sup>2</sup>, used for positioning, is sufficient to obtain centimetre accuracy.

In practice, the excellent performance obtained in this paper will be degraded by system imperfections, such as the differences in dc-offsets at the transmitter and receiver, and imperfections in the sizes, shapes and positions of the PDs and the apertures. In this paper, we already considered a solution to deal with the unknown dc-offset at the transmitter. By correlating the received signals with the carrier component of the transmitted signal (i.e., Case 2), the unknown dc-component is removed from the signal, at the cost of a slight reduction of the position accuracy. With respect to the other system impairments, we expect that the resulting accuracy will be of the same order of magnitude as UWB suffering from multipath interference (i.e. better than 10 cm), which is an order of magnitude better than the position accuracy that can be obtained with WiFi or BLE solutions (i.e. 2–3 m).

#### APPENDIX

In this appendix, we derive the FIM of the receiver position  $\boldsymbol{\theta} = (x_U, y_U)$ , based on the observation  $\mathbf{r}$  (2). Taking into account that  $\mathbf{r}|\boldsymbol{\theta} \sim N(R_p \tilde{\mathbf{H}}\boldsymbol{\mu}, \frac{N_0}{2} \tilde{\mathbf{R}})$ ,  $\ln p(\mathbf{r}|\boldsymbol{\theta})$  can be written as

$$\ln p(\mathbf{r}|\boldsymbol{\theta}) = C - \frac{1}{N_0} (\mathbf{r} - R_p \tilde{\mathbf{H}}\boldsymbol{\mu})^T \tilde{\mathbf{R}}^{-1} (\mathbf{r} - R_p \tilde{\mathbf{H}}\boldsymbol{\mu}), \quad (26)$$

where  $C$  is an irrelevant constant. Hence, the element  $(a, b)$  of the FIM, i.e.  $(\mathbf{F}_U)_{ab}$  can be written as

$$\begin{aligned} (\mathbf{F}_U)_{ab} &= E_{\mathbf{r}} \left[ \left( \frac{\partial}{\partial a} \ln p(\mathbf{r}|\boldsymbol{\theta}) \right) \left( \frac{\partial}{\partial b} \ln p(\mathbf{r}|\boldsymbol{\theta}) \right)^T \right] \\ &= \frac{2R_p^2}{N_0} \boldsymbol{\mu}^T \left( \frac{\partial}{\partial a} \tilde{\mathbf{H}} \right)^T \tilde{\mathbf{R}}^{-1} \left( \frac{\partial}{\partial b} \tilde{\mathbf{H}} \right) \boldsymbol{\mu}. \end{aligned} \quad (27)$$

Taking into account that

$$\frac{\partial}{\partial a} \tilde{\mathbf{H}} = \begin{pmatrix} \frac{\partial}{\partial a} \mathbf{H} & \mathbf{0} & \dots & \mathbf{0} \\ \mathbf{0} & \frac{\partial}{\partial a} \mathbf{H} & \dots & \mathbf{0} \\ \vdots & \vdots & \ddots & \vdots \\ \mathbf{0} & \mathbf{0} & \dots & \frac{\partial}{\partial a} \mathbf{H} \end{pmatrix} \quad (28)$$

and

$$\tilde{\mathbf{R}}^{-1} = \begin{pmatrix} (\mathbf{R}_{\psi}^{-1})_{1,1} \mathbf{I}_M & \dots & (\mathbf{R}_{\psi}^{-1})_{1,L} \mathbf{I}_M \\ \vdots & & \vdots \\ (\mathbf{R}_{\psi}^{-1})_{L,1} \mathbf{I}_M & \dots & (\mathbf{R}_{\psi}^{-1})_{L,L} \mathbf{I}_M \end{pmatrix}, \quad (29)$$

it follows that  $(\mathbf{F}_U)_{ab}$  (27) can be rewritten as

$$(\mathbf{F}_U)_{ab} = \frac{2R_p^2}{N_0} \sum_{\ell, \ell'=1}^K (\mathbf{R}_{\psi}^{-1})_{\ell, \ell'} \boldsymbol{\mu}_{\ell}^T \mathbf{X}^{ab} \boldsymbol{\mu}_{\ell'} \quad (30)$$

where  $\mathbf{X}^{ab}$  is defined in (11). Defining  $(\mathbf{W}^{ab})_{\ell, \ell'} = \boldsymbol{\mu}_{\ell}^T \mathbf{X}^{ab} \boldsymbol{\mu}_{\ell'}$ , and taking into account that  $\text{trace}(\mathbf{R}_{\psi}^{-1} \mathbf{W}^{ab}) = \sum_{\ell, \ell'=1}^L (\mathbf{R}_{\psi}^{-1})_{\ell, \ell'} (\mathbf{W}^{ab})_{\ell, \ell'}$ , we obtain (9).

#### REFERENCES

- [1] T. Komine and M. Nakagawa, "Performance evaluation of visible-light wireless communication system using white LED lightings," in *Proc. 9th Symp. Comput. Commun.*, Alexandria, Egypt, Jun. 2004, pp. 258–263.
- [2] J. Armstrong, Y. A. Sekercioglu, and A. Neild, "Visible light positioning: A roadmap for international standardisation," *IEEE Commun. Mag.*, vol. 51, no. 12, pp. 68–73, Dec. 2013.
- [3] S. Hann, J.-H. Kim, S.-Y. Jung, and C.-S. Park, "White LED ceiling lights positioning systems for optical wireless indoor applications," in *Proc. 36th Eur. Conf. Exhib. Opt. Commun.*, Torino, Italy, Sep. 2010, pp. 1–3.
- [4] S.-Y. Jung, S. Hann, and C.-S. Park, "TDOA-based optical wireless indoor localization using LED ceiling lamps," *IEEE Trans. Consum. Electron.*, vol. 57, no. 4, pp. 1592–1597, Nov. 2011.
- [5] K. Panta and J. Armstrong, "Indoor localization using white LEDs," *Electron. Lett.*, vol. 48, no. 4, pp. 228–230, Feb. 2012.
- [6] A. Arafat, X. Jin, and R. Klukas, "Wireless indoor optical positioning with a differential photosensor," *IEEE Photon. Technol. Lett.*, vol. 32, no. 14, pp. 2480–2485, Jul. 2012.
- [7] S.-Y. Jung, S. Hann, S. Park, and C.-S. Park, "Optical wireless indoor positioning system using light emitting diode ceiling lights," *Microw. Opt. Technol. Lett.*, vol. 54, no. 7, pp. 1622–1626, Jul. 2012.
- [8] M. Rahaim, G. B. Prince, and T. D. C. Little, "State estimations and motion tracking for spatially diverse VLC networks," in *Proc. Globecom Workshops*, Anaheim, CA, USA, Dec. 2012, pp. 1249–1253.

- [9] H.-S. Kim, D.-R. Kim, S.-H. Yang, Y.-H. Son, and S.-K. Han, "An indoor visible light communication positioning system using a RF allocation technique," *J. Lightw. Technol.*, vol. 31, no. 1, pp. 134–144, Jan. 2013.
- [10] U. Nadeem, N. U. Hassan, M. A. Pasha, and C. Yuen, "Highly accurate 3D wireless indoor positioning system using white LED lights," *Electron. Lett.*, vol. 50, no. 11, pp. 828–830, May 2014.
- [11] G. Kail, P. Maechler, N. Preyss, and A. Burg, "Robust asynchronous indoor localization using LED lighting," *Proc. IEEE Int. Conf. Acoust., Speech Signal Process.*, Florence, Italy, May 2014, pp. 1866–1870.
- [12] S.-H. Yang, H.-S. Kim, Y.-H. Son, and S.-K. Han, "Three-dimensional visible light indoor localization using AOA and RSS with multiple optical receivers," *J. Lightw. Technol.*, vol. 32, no. 14, pp. 2480–2485, Jul. 2014.
- [13] T. Q. Wang, C. He, and J. Armstrong, "Angular diversity for indoor MIMO optical wireless communications," in *Proc. IEEE Int. Conf. Commun.*, London, U.K., Jun. 2015, pp. 5066–5071.
- [14] X. Zhang, J. Duan, Y. Fu, and A. Shi, "Theoretical accuracy analysis of indoor visible light communication positioning system based on received signal strength indicator," *J. Lightw. Technol.*, vol. 32, no. 21, pp. 3578–3584, Nov. 2014.
- [15] A. Sahin, Y. S. Eroglu, I. Guvenc, N. Pala, and M. Yuksel, "Hybrid 3D localization for visible light communication systems," *J. Lightw. Technol.*, vol. 33, no. 22, pp. 4589–4599, Nov. 2015.
- [16] T. Q. Wang, Y. A. Sekercioglu, A. Neild, and J. Armstrong, "Position accuracy of time-of-arrival based ranging using visible light with application in indoor localization systems," *J. Lightw. Technol.*, vol. 31, no. 20, pp. 3302–3308, Oct. 2013.
- [17] H. Steendam, T. Q. Wang, and J. Armstrong, "Cramer-Rao bound for indoor visible light positioning using an aperture-based angular diversity receiver," in *Proc. IEEE Int. Conf. Commun.*, Kuala Lumpur, Malaysia, Jun. 2016, pp. 1–6.
- [18] J. M. Kahn and J. R. Barry, "Wireless infrared communications," in *Proc. IEEE*, vol. 85, no. 2, pp. 265–298, Feb. 1997.
- [19] H. L. Van Trees, "Detection, Estimation, and Modulation Theory," New York, NY, USA: Wiley, 1968.
- [20] J. B. Carruthers and J. M. Kahn, "Multiple-subcarrier modulation for nondirected wireless infrared communication," *IEEE J. Sel. Areas Commun.*, vol. 14, no. 3, pp. 538–546, Mar. 1996.
- [21] O. Gonzalez *et al.*, "OFDM over indoor wireless optical channel," *Proc. Inst. Elect. Eng.—Optoelectron.*, vol. 152, no. 4, pp. 199–204, Aug. 2005.
- [22] N. U. Hassan, A. Naeem, M. A. Pasha, and C. Yuen, "Indoor positioning using visible LED lights: A survey," *ACM Comput. Surveys*, vol. 48, no. 2, pp. 20.1–20.32, Nov. 2015.
- [23] M. Aminikashani, W. Gu, and M. Kavehrad, "Indoor location estimation with optical-based orthogonal frequency division multiplexing communications," *Opt. Eng.*, vol. 55, no. 5, May 2016, Art. no. 056116. doi: 10.1117/1.OE.55.5.056116.
- [24] E.-M. Jeong, S.-H. Yang, H.-S. Kim, and S.-K. Han, "Tilted receiver angle error compensated indoor positioning system based on visible light communication," *Electron. Lett.*, vol. 49, no. 14, pp. 890–891, Jul. 2013.
- [25] L. Zeng *et al.*, "High data rate multiple input multiple output (MIMO) optical communications using white LED lighting," *IEEE J. Sel. Areas Commun.*, vol. 27, no. 9, pp. 1654–1662, Dec. 2009.
- [26] O. Bouchet, *Wireless Optical Telecommunications*, New York, NY, USA: Wiley, 2012.

**Heidi Steendam** (M'01–SM'06) received the M.Sc. degree in electrical engineering and the Ph.D. degree in applied sciences from Ghent University, Gent, Belgium, in 1995 and 2000, respectively.

Since September 1995, she has been with the Digital Communications Research Group, Department of Telecommunications and Information Processing, Faculty of Engineering, Ghent University, first in the framework of various research projects, and since October 2002 as a full-time Professor of digital communications. She is the author of more than 140 scientific papers in international journals and conference proceedings, for which she received several best paper awards. Her main research interests include statistical communication theory, carrier and symbol synchronization, bandwidth-efficient modulation and coding, cognitive radio, and cooperative networks and positioning.

Since 2002, Dr. Steendam has been an executive Committee Member of the IEEE Communications and Vehicular Technology Society Joint Chapter, Benelux Section, and since 2012 the Vice-Chair. She has been active in various international conferences as Technical Program Committee Chair/Member and Session Chair. In 2004 and 2011, she was the Conference Chair of the IEEE Symposium on Communications and Vehicular Technology in the Benelux. She is currently an Associate Editor of the IEEE TRANSACTIONS ON COMMUNICATIONS and the *EURASIP Journal on Wireless Communications and Networking*.

**Thomas Qian Wang** received the B.E. degree in electric engineering from Dalian Jiaotong University, Dalian, China, in 2006, and the M.E. and Ph.D. degrees in communication and information systems from Dalian Maritime University, Dalian, in 2008 and 2011, respectively. From March 2012 to December 2015, he was a Research Fellow with the Department of Electrical and Computer Systems Engineering, Monash University, Melbourne, Vic, Australia. He is currently a Research Fellow with the Global Big Data Technologies Centre, University of Technology Sydney, Sydney, NSW, Australia. His research interests include optical wireless communications and multiple-input multiple-output (MIMO) technology.

**Jean Armstrong** (M'90–SM'06–F'15) was born in Scotland. She received the B.Sc. (First Class Hons.) degree in electrical engineering from the University of Edinburgh, Edinburgh, U.K., and the M.Sc. degree in digital techniques from Heriot-Watt University, Edinburgh.

She is currently a Professor at Monash University, Melbourne, Vic, Australia, where she leads a research group working on topics including optical wireless, radio frequency, and optical fiber communications. She has published numerous papers including more than 70 on aspects of OFDM for wireless and optical communications and has six commercialized patents. Before emigrating to Australia, she was a Design Engineer at Hewlett-Packard, Ltd., Scotland. In Australia, she has held a range of academic positions at Monash University, the University of Melbourne, and La Trobe University. She received numerous awards including a Carolyn Haslett Memorial Scholarship, a Zonta Amelia Earhart Fellowship, the Peter Doherty Prize for the best commercialization opportunity in Australia (joint winner), induction into the Victorian Honour Roll of Women, the 2014 IEEE Communications Society Best Tutorial Paper Award, and the 2016 IET Mountbatten Medal. She is currently a Fellow of the IEAust. She was on the Australian Research Council (ARC) College of Experts and the ARC Research Evaluation Committee. She is currently an Associate Editor of the IEEE TRANSACTIONS ON COMMUNICATIONS and the *Journal of Optical Communications and Networking*.